

Article

Experimental and Numerical Investigations on the Impact of Surface Conditions on Self-Piercing Riveted Joint Quality

Huan Zhao ^{1,2} , Li Han ³, Yunpeng Liu ^{4,*} and Xianping Liu ^{5,*}

- ¹ School of Mechanical Engineering, Tianjin University of Science and Technology, Tianjin 300222, China; zhaohuan@tust.edu.cn
- ² Tianjin Key Laboratory of Integrated Design and Online Monitoring of Light Industry and Food Engineering Machinery and Equipment, Tianjin 300222, China
- ³ Hansher Consulting Ltd., Coventry CV3 2UB, UK
- ⁴ Shanghai Key Laboratory of Digital Manufacture for Thin-Walled Structures, School of Mechanical Engineering, Shanghai Jiao Tong University, Shanghai 200240, China
- ⁵ School of Engineering, University of Warwick, Coventry CV4 7AL, UK
- * Correspondence: yunpeng-liu@sjtu.edu.cn (Y.L.); x.liu@warwick.ac.uk (X.L.)

Abstract: In this study, experimental and numerical investigations were carried out to achieve a comprehensive understanding of the impact of surface conditions on self-piercing riveting (SPR) joint quality. Oil lubrication and sandpaper grinding were employed in experimental tests to change surface conditions at rivet/top sheet, top/bottom sheets and bottom sheet/die interfaces. A finite element (FE) model for the SPR process was also adopted to numerically assess the impact of surface conditions. Variations in surface conditions were modelled by changing friction coefficients at contact interfaces. The results revealed that the friction coefficient between the rivet and top sheet (μ_1) imposed significant influences on the interlock (I_1) by affecting the deformation of the rivet shank and top sheet. The friction coefficient between the rivet and bottom sheet (μ_2) showed a lower influence on the joint quality because of a smaller contact area and shorter interaction time. The friction coefficient between the top and bottom sheets (μ_3) led to opposite changing trends of remaining bottom sheet thickness at the joint centre (t_c) and under the rivet tip (t_{tip}). The friction coefficient between the bottom sheet and die (μ_4) demonstrated crucial influences on the remaining bottom sheet at the joint centre. The riveting force was significantly influenced throughout the whole riveting process by the μ_1 , but only affected at the end of the joining process by the other three friction coefficients.

Keywords: self-piercing riveting; surface condition; friction coefficient; joint quality; FE model



Citation: Zhao, H.; Han, L.; Liu, Y.; Liu, X. Experimental and Numerical Investigations on the Impact of Surface Conditions on Self-Piercing Riveted Joint Quality. *Coatings* **2023**, *13*, 858. <https://doi.org/10.3390/coatings13050858>

Academic Editor:
Diego Martinez-Martinez

Received: 29 March 2023
Revised: 18 April 2023
Accepted: 28 April 2023
Published: 30 April 2023



Copyright: © 2023 by the authors. Licensee MDPI, Basel, Switzerland. This article is an open access article distributed under the terms and conditions of the Creative Commons Attribution (CC BY) license (<https://creativecommons.org/licenses/by/4.0/>).

1. Introduction

The 5xxx and 6xxx series aluminium alloys have been intensively used in car body-in-white (BIW) structures in recent years. As a mechanical joining approach, self-piercing riveting (SPR) has become the major joining technique for these lightweight alloys and has been widely adopted by automobile companies, such as Audi [1], Jaguar Land Rover (JLR) [2] and BMW [3]. It is suitable for high-ductility materials, and can also be extended to join low-ductility materials such as high-strength steels [4]. Figure 1a shows the four steps of the SPR process, namely clamping, piercing, flaring and tool releasing. Three indicators are usually measured on the SPR joint cross-sectional profile to evaluate the joint quality, as shown in Figure 1b, namely the rivet head height (H_1), interlock (I_1) and minimum remaining bottom sheet thickness (T_{min}). The quality standard of these indicators varies in different industry sectors or even companies. For instance, according to the criterion of a world-leading car maker, the H_1 should be -0.5 to 0.3 mm and the I_1 must be larger than 0.4 mm for aluminium alloy joints. The T_{min} should be no less than 0.2 mm [5]. The H_1 can be conveniently controlled by adjusting punch displacement in the riveting system, whilst the I_1 and T_{min} are directly influenced by plastic deformation of the rivet and sheets [6].

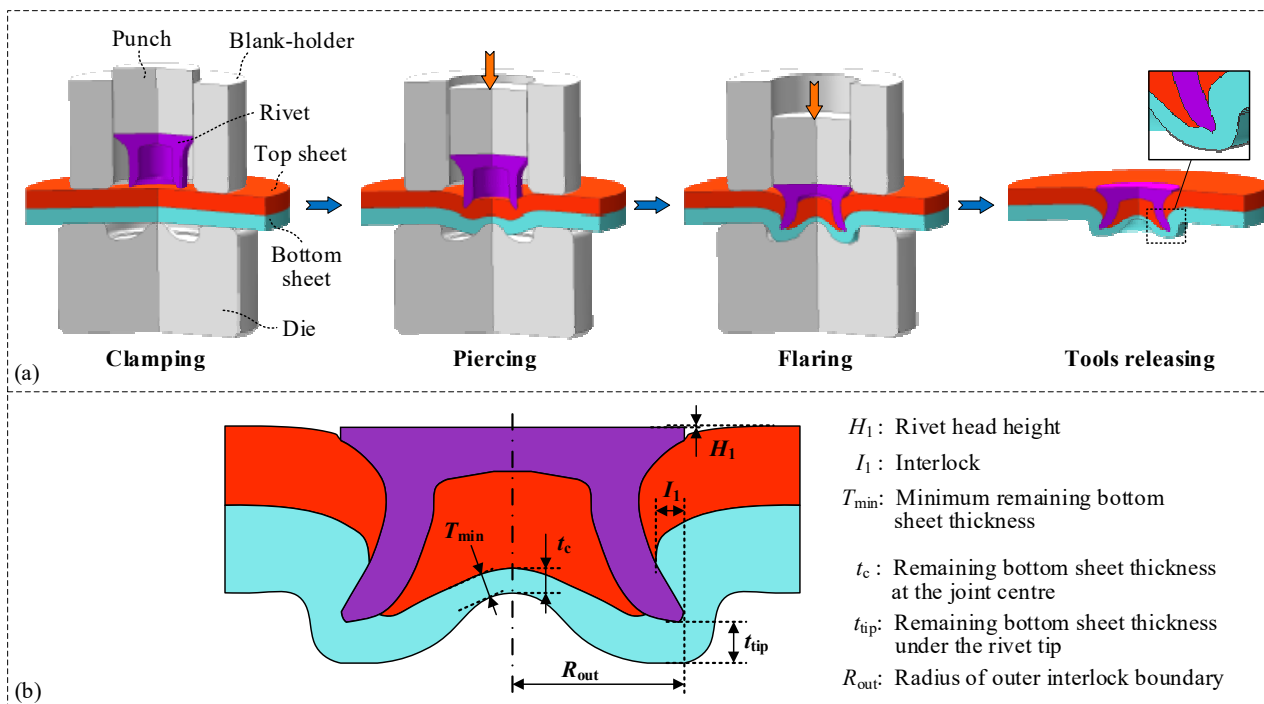


Figure 1. Schematic of (a) self-piercing riveting process and (b) indicators measured on joint cross-sectional profile.

Factors affecting the deformation behaviours of rivets and sheets will inevitably influence the formation processes and magnitudes of I_1 and T_{min} . The rivet property and die profile are two critical factors determining the I and T_{min} , and their impacts such as rivet hardness, rivet material, die depth and die diameter have been investigated in the literature [5]. Aside from rivet and die parameters, the formation of the I and T_{min} are also affected by the surface conditions of the rivet, sheets and die. To successfully punch the rivet into sheets, a high riveting force (20~70 kN) is usually required in the SPR process [7], which leads to strong interaction forces among multiple touching components. Variations in surface conditions will directly alter the friction coefficient at the contact interface and influence the magnitude of friction force [8]. As a result, the deformation behaviours of the rivet and sheets will be unavoidably affected [9], and the final joint quality will also be influenced, as shown in Figure 2 [10].

Some efforts have been made to experimentally investigate the effects of surface conditions on SPR joint quality. Surface modification methods, including coating [11], polishing, grit blasting [10], impression [12] and lubricants [13], were adopted by researchers to change the surface conditions. By altering the bottom surface texture of the top sheet with different impression tools and garnet particles, Li [10] explored the influences of the interface condition between two AA5754 sheets on SPR joint quality. It was found that the local surface modification only slightly changed the magnitudes of joint quality indicators. The same author [12] further modified the contact interface conditions between sheets using hot water washing (around 60 °C), P120 sandpaper grinding and grit blasting. The results revealed that the hot water wash and sandpaper grinding did not show a significant influence on the joint quality. The grit blasting obviously resulted in a greater I_1 but a smaller T_{min} . Han et al. [11] experimentally studied the effects of different bottom sheet coatings (i.e., E-coating and zinc coating) on the quality of SPR joints with NG5754 top sheet and HSLA350 bottom sheet. The results showed that a larger I_1 but a smaller or even zero T_{min} were obtained due to the lubricating effect of coatings. Karim et al. [14] compared the influences of mechanically plated Zn-Sn-Al (Almac[®]) and electroplated Zn-Ni rivet coatings on SPR joint quality. It was found that the Zn-Ni rivet coating contributed to a greater I_1 compared to the Almac rivet coating. However, SPR joints with the Zn-Ni rivet

coating demonstrated lower lap-shear and cross-tensile strengths than those with the Almac rivet coating. These experimental studies extended the understanding of the influences of surface conditions on SPR joint quality. However, because of intrinsic variability of the SPR process (e.g., manufacturing tolerances of sheet thickness, rivet length and hardness), the experimentally measured quality indicators for the same joint configuration usually vary within a certain range. This makes it difficult to properly assess the influences of surface conditions on SPR joint quality.

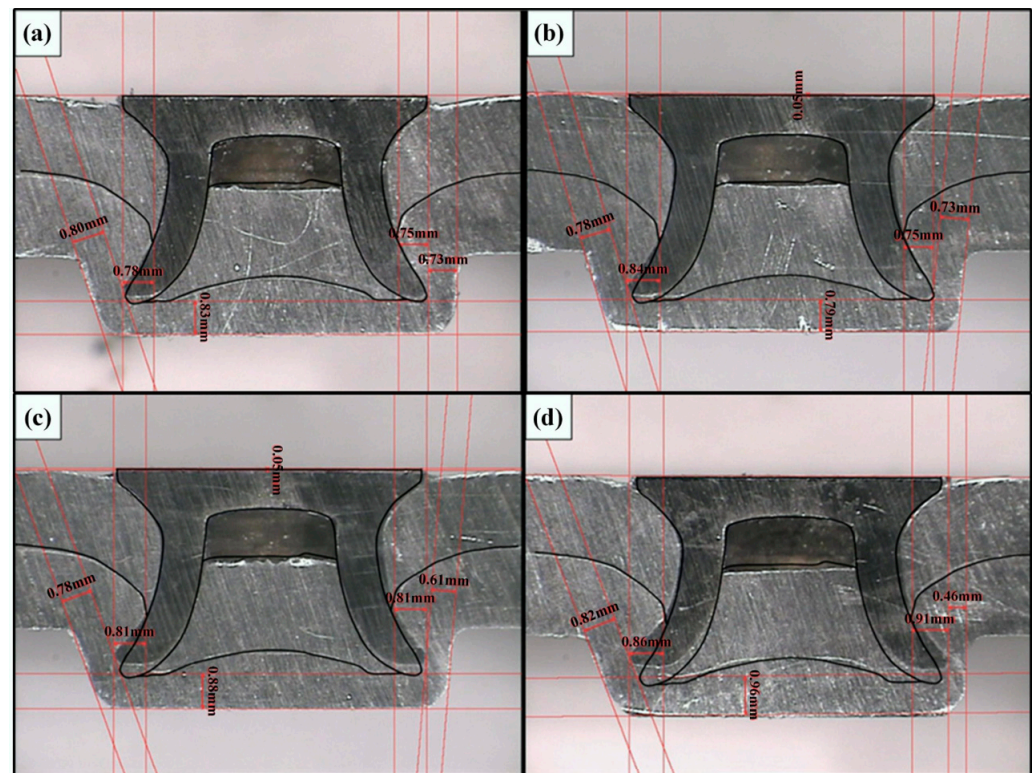


Figure 2. Cross-sectional profiles of (2 + 2 mm) AA5754 SPR joints with different surface conditions: (a) bottom surface of the top sheet modified by washing with hot tap water; (b) bottom surface of the top sheet modified by grinding with P120 sandpaper; (c) bottom surface of the top sheet modified by grit blasting; (d) bottom surface of the top sheet and top surface of the bottom sheet modified by grit blasting [10].

To overcome the disadvantages of the experimental approach, numerical analyses with a finite element (FE) model have also been conducted in some studies to explore the impact of surface conditions [15,16]. It has been widely proved that a properly calibrated FE model of the SPR process can accurately predict the riveting force [17], material deformation behaviour [18] and final joint quality [19]. More importantly, the FE model always gives a consistent simulation result for the same joint configuration. Variations in surface conditions can be conveniently represented by different magnitudes of friction coefficients at the contact interface. With the help of a three-dimensional (3D) FE model and design of experiment (DOE), Moraes et al. [20] evaluated the importance of friction coefficients at different contact interfaces in the SPR joint with magnesium alloy AM60 top sheet and aluminium alloy AA6082 bottom sheet. It was found that friction coefficients between the die and bottom sheet and between the rivet and top sheet had the most significant influences on the joint quality. Suitable friction coefficients for the studied SPR joints were also identified by proposing four multiple linear equations. Changing trends of joint quality indicators with different friction coefficients were not investigated in their study. With a 3D smoothed particle Galerkin (SPG) model in LS-DYNA/explicit, Huang et al. [21] also discussed the sensitivity of joint quality indicators to friction coefficients at different contact interfaces.

Han et al. [9] numerically studied the effects of friction coefficients on joint quality using a two-dimensional (2D) FE model of an SPR joint with a flat plate die. The results revealed that the friction coefficient between the blank-holder and top sheet (0.1~0.3) could affect the movements of sheets along the horizontal direction, while the friction coefficient between the rivet and sheets (0.1~0.3) had significant influences on the formation of I_1 and T_{\min} . The friction coefficient between the top and bottom sheets (0.3~0.5) directly influenced the appearance of gaps in the final joints. The friction coefficient between the bottom sheet and supporting plate (0.2~0.5) significantly affected the deformation of the bottom sheet and rivet shank. With a 2D FE model of the SPR process in MSC Marc, Jacek [22] found that the friction coefficient between the rivet and sheets (0.05~0.25) imposed apparent influences on the deformation behaviours of the rivet shank and top sheet. Similar conclusions were also reached by Hoang et al. [23]: the friction coefficient between the rivet and sheets significantly affected the plastic strain localisation on the rivet shank. Until now, there has not been a comprehensive study about the influences of surface conditions (or friction coefficients) on SPR joint formation and final quality.

In addition, to guide the design of new SPR joints, an in-depth understanding of surface conditions' impacts will also be helpful to speed up the FE model development for the SPR process. Although different experimental methods can be employed to measure friction coefficients at contact interfaces [10,24,25], the inverse method is still the most straightforward and effective way to determine friction coefficients when developing an FE model of the SPR process. Table 1 shows the friction coefficients implemented in FE models of the SPR process in recently published literature. A uniform friction coefficient was used between different contact parts in some FE models [26–28]. This can effectively reduce the difficulty of identifying the suitable friction coefficient with the inverse method. However, considering the different surface conditions at multiple contact interfaces, this simplification does not conform with the real conditions. To solve this problem, different friction coefficients were utilised at contact interfaces in other FE models [19,29,30]. This strategy improved the consistency between the FE model and the real SPR process but increased the difficulty of friction coefficient identification. Therefore, to facilitate and speed up friction coefficient identification, it is important to determine how friction coefficients at different contact interfaces affect the simulated joining process and final joint quality.

Table 1. Friction coefficients used in different FE models of the SPR process.

Authors	Model Type	Software	Friction Coefficients
Rusia and Weihe [29]	2D	LS-DYNA	0.12 between deformable parts 0.2 between tools and deformable parts
Wang et al. [26]	2D	DEFORM-2D	0.12 between all parts
Karathanasopoulos et al. [27]	2D	ABAQUS	0.2 between all parts
Hönsch et al. [30]	2D	Simufact.Forming	0.1 for rivet/sheets, 0.3 for sheets/die, 0.2 for others
Deng et al. [28]	2D	Simufact.Forming	0.2 between all parts
Moraes et al. [31]	3D	ABAQUS	0.4 for punch/rivet, 0.15 for others
AMRO et al. [32]	2D	ABAQUS	0.2 between all parts
Huang et al. [33]	3D	ABAQUS	0.2 between all parts
Hirsch et al. [34]	3D	ABAQUS	0.0 for composite sheet/rivet, 0.3 for others
Carandente et al. [19]	2D	Simufact.Forming	0.09 for top/bottom sheets, 0.15 for bottom sheet/die, 0.15 for top sheet/blank-holder
He et al. [35]	2D	LS-DYNA	0.15 for top sheet/blank-holder, 0.15 for top/bottom sheets, 0.25 for others

In this research, experimental SPR tests were carried out to evaluate the influences of different surface conditions on joint quality. Oil lubrication and sandpaper grinding were employed to change the surface conditions at the rivet/top sheet interface, top/bottom sheet interface and bottom sheet/die interface. Meanwhile, a verified simulation model of the SPR process was adopted to systematically assess the impact of surface conditions.

Variations in surface conditions were modelled by changing friction coefficients at four critical contact interfaces. Influences of surface conditions on joint quality and deformation of rivets and sheets were also numerically analysed. This study is beneficial for a better understanding of how surface conditions affect the SPR joining results and provides guidelines on how to improve the joint quality by optimising surface conditions in practice. The results of this study are also helpful for the fast identification of friction coefficients when developing an FE model for the SPR process.

2. Experimental Setup

2.1. Rivet and Sheet Materials

The aluminium alloy AA5754 provided by Jaguar Land Rover (JLR) was used for the top and bottom sheets, and its mechanical properties and composition are listed in Table 2. Semi-tubular rivets were made of boron steel with hardness 280 ± 30 HV10 and manufactured by Tucker GmbH.

Table 2. Mechanical properties and composition of AA5754 (Reprinted with permission from [36]).

Mechanical Properties	Young's Modulus (GPa)	Tensile Strength (MPa)	Elongation (%)	Hardness (HV)	
	70	240	22	63.5	
Nominal composition (wt%)	Si 0~0.40	Fe 0~0.40	Cu 0~0.10	Mn 0~0.50	Mg 2.60~3.60

2.2. Experiment Design

As shown in Figure 3a, the SPR system manufactured by Tucker GmbH was employed throughout the experiment. The riveting speed and clamping force were 300 mm/s and 6.0 kN, respectively. The thicknesses of the top sheet and bottom sheet were 1.8 mm and 2.0 mm, respectively. To study the influences of surface conditions on the joint quality, three critical contact interfaces in Figure 3b were modified, namely interfaces between the rivet and top sheet (blue line), between the top and bottom sheets (green line) and between the bottom sheet and die (red line). Two surface modification approaches were utilised, namely oil lubrication to reduce the friction coefficient and P200 sandpaper grinding to increase the friction coefficient. In order to ensure the same surface conditions in repeated tests as much as possible, the same amount of low-viscosity lubricating oil was applied evenly on the sheet surface. A thin layer of oil was formed at the contact interface and thus effectively reduced the friction coefficient. The same P200 sandpaper was used to manually grind the sheet surface for five minutes, which resulted in a higher surface roughness and therefore a greater friction coefficient at the contact interface. The grinding speed and applied force were controlled the same as much as possible to ensure the consistency of the grinding process. As listed in Table 3, six groups of SPR joints with different surface conditions were therefore manufactured. A uniformed specimen shape (i.e., 40 mm × 40 mm in Figure 4a) was used to eliminate possible influences of sheet dimensions on the joint formation and final quality. According to the sheet configuration, 6.0 mm long semi-tubular rivets and a pip die were selected. The nominal dimensions of the rivet and die are illustrated in Figure 4b,c. To facilitate the joining result comparison, the rivet head height (H_1) in all SPR joints was set to 0.0 mm by controlling the rivet displacement. Three repeats for each joint group were performed.

All of the SPR joints were cut along the joint central plane using an abrasive-wheel cutting machine. For the 40 mm × 40 mm specimen, specially designed fixtures were used in the riveting and cutting processes to ensure the cutting plane was as close as possible to the joint central plane [37]. The sectioned joints were polished, and the cross-sectional profile for each joint was inspected using an optical microscope. Although H_1 , I_1 and T_{\min} are widely adopted to assess SPR joint quality, they are insufficient to accurately describe the changing trends of joint formation, rivet shank deformation and remaining bottom sheet thickness distribution because the T_{\min} is the minimum remaining bottom sheet

and its position changes from joint to joint. The rivet shank deformation behaviour is critical for the final joint quality, but cannot be directly evaluated by any of the three quality indicators. Therefore, to overcome this difficulty, three dimensions were measured on the cross-sectional profile to evaluate the joint formation and final quality, namely the I_1 and the remaining bottom sheet thickness at the joint centre (t_c) and under the rivet tip (t_{tip}), as shown in Figure 1b. The radius of the outer interlock boundary (R_{out}) was also extracted to assess the rivet shank deformation.

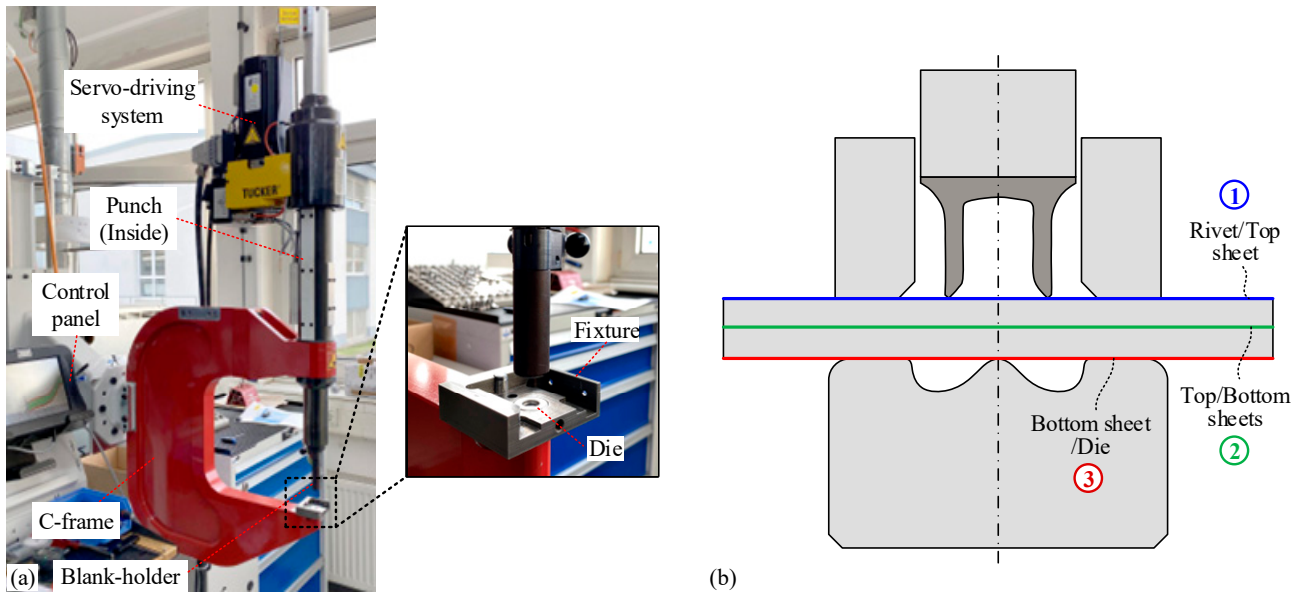


Figure 3. (a) Structure of the Tucker SPR system and (b) three critical contact interfaces between rivet, sheets and die.

Table 3. Joint configurations in experimental SPR tests.

Joint No.	Thickness (mm)		Rivet (Boron Steel)	Die	Contact Interface	Surface Modification Method
	Top Sheet/ T_t (AA5754)	Bottom Sheet/ T_b (AA5754)				
1-1					Rivet/top sheet	Oil lubrication
1-2						Sandpaper grinding
2-1					Top/bottom sheet	Oil lubrication
2-2	1.8	2.0	C5.3*6.0 (280 ± 30 HV10)	Pip die		Sandpaper grinding
3-1					Bottom sheet/die	Oil lubrication
3-2						Sandpaper grinding

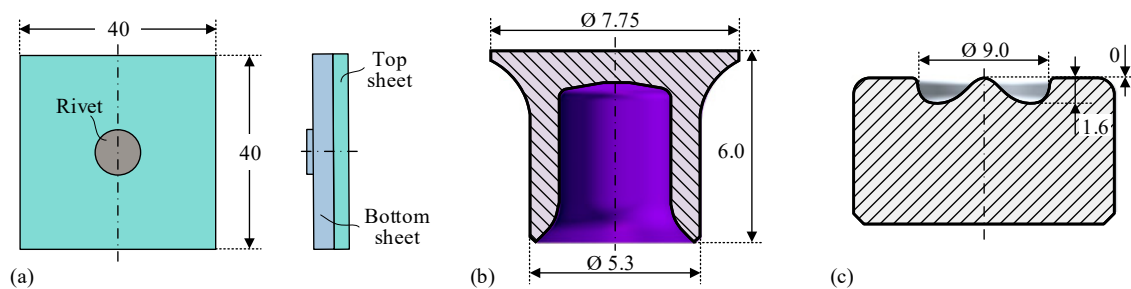


Figure 4. Dimensions of (a) specimen, (b) semi-tubular rivet and (c) pip die (in mm).

3. Finite Element (FE) Model

3.1. Model Description

To systematically investigate the influences of surface conditions at different interfaces, a previously developed [38] and validated 2D FE model of the SPR process was adopted as shown in Figure 5a. Commercial software Simufact.Forming 15 was employed due to its strong re-meshing capability. The sheet edges could freely move while all the freedoms of the die were fixed during the riveting process. A 5.3 kN clamping force was applied on the blank-holder to clamp the top and bottom sheets together. The punch had a constant speed ($v_1 = 300 \text{ mm/s}$) and moved downward to press the rivet into the sheets. The boron steel rivet and AA5754 sheets were modelled as elastic-plastic bodies, while the punch, blank-holder and die were modelled as rigid bodies. Plastic stress-strain curves for the AA5754 and the boron steel are shown in Figure 5b,c. The temperature effect on the material properties was only considered for the AA5754 sheets but not considered for the boron steel rivet. This is because the maximum temperature within the joining region is usually lower than $250 \text{ }^\circ\text{C}$ [19] and imposes limited influences on the mechanical properties of the boron steel. Uniaxial tensile tests at four different temperatures were carried out to determine the plastic stress-strain curves for the AA5754 sheets, whilst only the uniaxial tensile test at room temperature was performed to obtain the plastic stress-strain curve for the boron steel rivet. All the deformable parts were meshed using the quad element with four Gauss points, and the global mesh sizes for the rivet, top sheet and bottom sheet were 0.10 mm , 0.10 mm and 0.12 mm , respectively. The automatic re-meshing technique was used to deal with mesh distortion caused by large plastic deformations of the two sheets. A geometrical criterion was implemented to model the blanking of the top sheet [19], and the critical thickness was set to 0.04 mm . The Coulomb friction model was selected, and the inverse method was adopted to identify friction coefficients between different parts. The friction coefficient between the die and bottom sheet was set to 0.22 , while that between other solid parts was set to 0.10 . To ensure efficiency, the springback of SPR joints during the tool (i.e., punch, blank-holder and die) releasing process was not simulated. More details about the FE model can be found in [38]. Other boundary conditions were kept consistent with those in experimental tests.

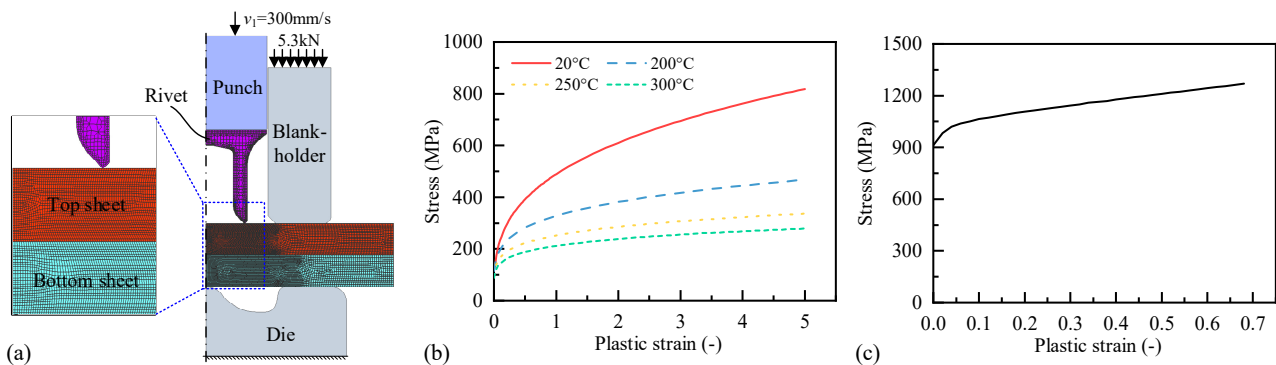


Figure 5. (a) FE model, (b) stress-strain curves of AA5754 (strain rate = 1 s^{-1}) [19] and (c) stress-strain curves of boron steel (strain rate = 0.01 s^{-1}).

3.2. Simulation Design

By changing the magnitude of the friction coefficient, the impacts of surface conditions at four critical contact interfaces on the riveting process and final joint quality were numerically investigated. Considering the difficulty of solely changing surface conditions at the rivet/bottom sheet interface in experimental tests, the impact of surface conditions at the rivet/bottom sheet interface was only numerically investigated in this research. Figure 6 shows the positions of four critical interfaces and corresponding friction coefficients: (1) between the rivet and top sheet (μ_1); (2) between the rivet and bottom sheet (μ_2); (3) between the top and bottom sheets (μ_3); and (4) between the bottom sheet and die (μ_4). Influences

of surface conditions at other interfaces are not discussed in this study considering their lower impact on the joining results [20]. The initial FE model setup was regarded as the benchmark. Six levels (i.e., 0.01, 0.1, 0.2, 0.3, 0.4 and 0.5) of each friction coefficient were selected to represent different surface conditions, such as oil lubrication and sandpaper grinding. This variation range of friction coefficients covers the values of friction coefficients used in FE models in the accessible literature [26,27,29,30]. For consistency, all the simulations were terminated when the H_1 was reduced to 0.0 mm. The simulated joint cross-sectional profile, three quality indicators (i.e., I_1 , t_c and t_{tip}) and force-displacement curve were extracted and analysed in detail.

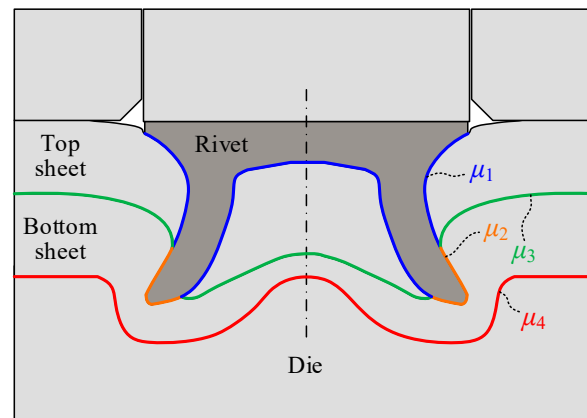


Figure 6. Schematic of friction coefficients at four critical interfaces.

4. Results and Discussion

4.1. Experimental Results

Cross-sectional profiles of SPR joints listed in Table 3 were experimentally captured as shown in Figure 7. It can be noticed that the joint profile is not exactly symmetrical, which might be caused by a slight misalignment between the die and punch axis or by deflection of the C-frame in the SPR system. Through visual observation, it is difficult to identify the differences among these profiles. To quantitatively assess the impact of surface condition on joint quality, mean values of the I_1 , t_{tip} and R_{out} on the left and right sides were calculated and plotted into histograms. For easier description, the oil-lubricated and sandpaper-ground surfaces are regarded as surfaces with low and high friction coefficients, respectively. Slightly smaller I_1 , t_{tip} and R_{out} but greater t_c were achieved with a high friction coefficient at the rivet/top sheet interface, as shown in Figure 8a. Obviously smaller I_1 , t_c and R_{out} but greater t_{tip} were generated with a high friction coefficient at the top/bottom sheet interface, as shown in Figure 8b. Slightly smaller t_{tip} and R_{out} but greater I_1 and t_c were achieved with a high friction coefficient at the bottom sheet/die interface, as shown in Figure 8c. These results indicate that lower friction coefficients at the rivet/top sheet interface and top/bottom sheet interface but a higher friction coefficient at the bottom sheet/die interface can contribute to a larger I_1 . Higher friction coefficients at rivet/top sheet interface and bottom sheet/die interface but a lower friction coefficient at top/bottom sheet interface can contribute to a larger t_c but a smaller t_{tip} . Lower friction coefficients at three contact interfaces can always lead to a greater R_{out} .

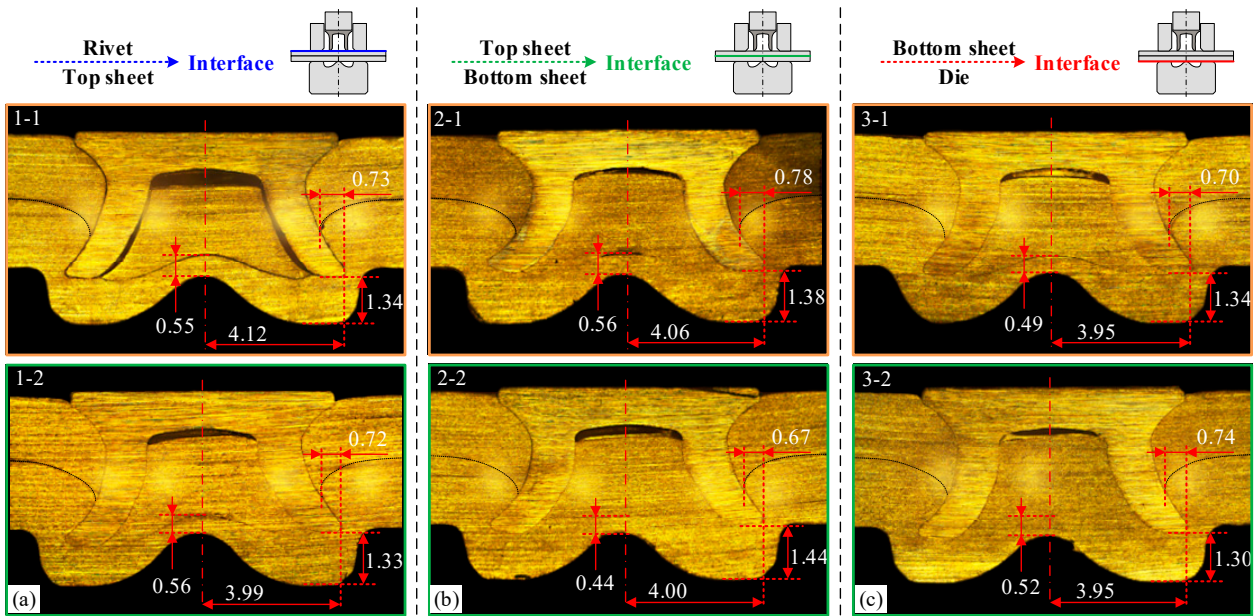


Figure 7. Joint cross-sectional profiles with different surface conditions between (a) rivet/top sheet, (b) top/bottom sheets and (c) bottom sheet/die (in mm).

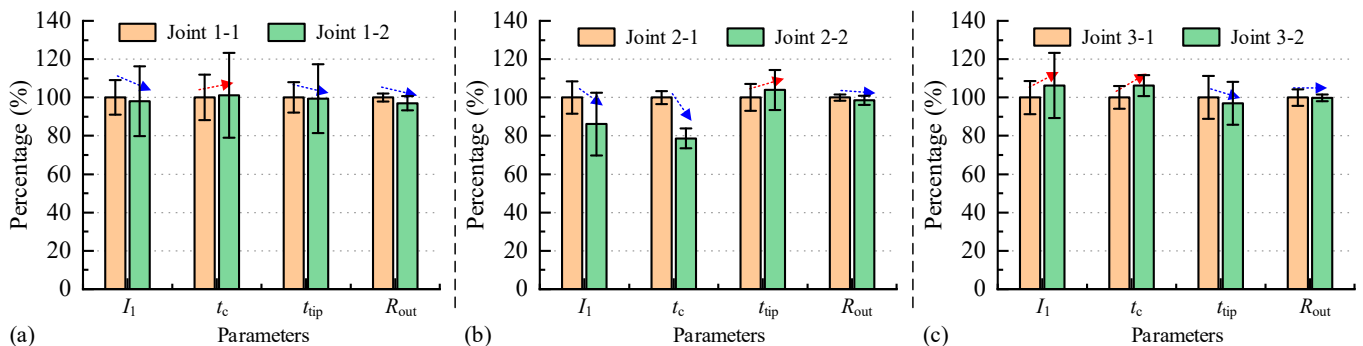


Figure 8. Variations in quality indicators with different surface conditions between (a) rivet/top sheet, (b) top/bottom sheets and (c) bottom sheet/die.

4.2. FE Model Validation

Considering the similar cross-sectional profiles and close qualities of six SPR joints (see Figures 7 and 8), the experimental result of joint 1-2 was selected to confirm the effectiveness of the FE model employed in this research. Figure 9 shows the experimentally tested and simulated joint cross-sectional profiles, four indicators (i.e., I_1 , R_{out} , t_c and t_{tip}) and force-displacement curves. It can be seen from Figure 9a that the simulated cross-sectional profile showed a reasonable agreement with the experimentally tested one: the deformed shapes of rivet shank and sheets were accurately predicted. In Figure 9b, it can be seen that the simulated I_1 , t_c and R_{out} were 89% (0.72 mm vs. 0.64 mm), 99% (0.56 mm vs. 0.55 mm) and 96% (3.99 mm vs. 3.83 mm) of the tested ones, respectively, but the simulated t_{tip} was only 70% (1.33 mm vs. 0.93 mm) of the tested one. The prediction accuracies for the I_1 , t_c and R_{out} are 19%~29% higher than that for the t_{tip} in joint 1-2. In previous research [38], this FE model had also been validated by comparing the experimental and simulation results of eleven joints within the same studied range, and the mean absolute error (MAE) for the I_1 , t_c and t_{tip} was 0.066 mm, 0.042 mm and 0.115 mm, respectively, and the corresponding mean absolute percentage error (MAPE) was 10.5%, 12.9% and 19.7%. Overall, the prediction result of the FE model for these joint quality indicators is accurate. The force-displacement curve was also accurately predicted by the FE model: not only the variation trend but also

the magnitude of riveting force was accurately predicted, as shown in Figure 9c, except for a small drop presented on the simulated force-displacement curve. This is because a geometrical criterion was implemented to model the blanking of the top sheet [19], and the critical thickness was set to 0.04 mm. When the remaining top sheet thickness is equal to or smaller than the critical thickness value, the sheet elements underneath the rivet tip will be deleted from the FE model to represent the top sheet fracture. Thus, the force decreases suddenly to some extent, and a small drop appears on the force-displacement curve. Overall, the employed FE model can give a reasonable prediction result for the studied SPR joint, and thus it was utilised to numerically investigate the impacts of different surface conditions on the joining results.

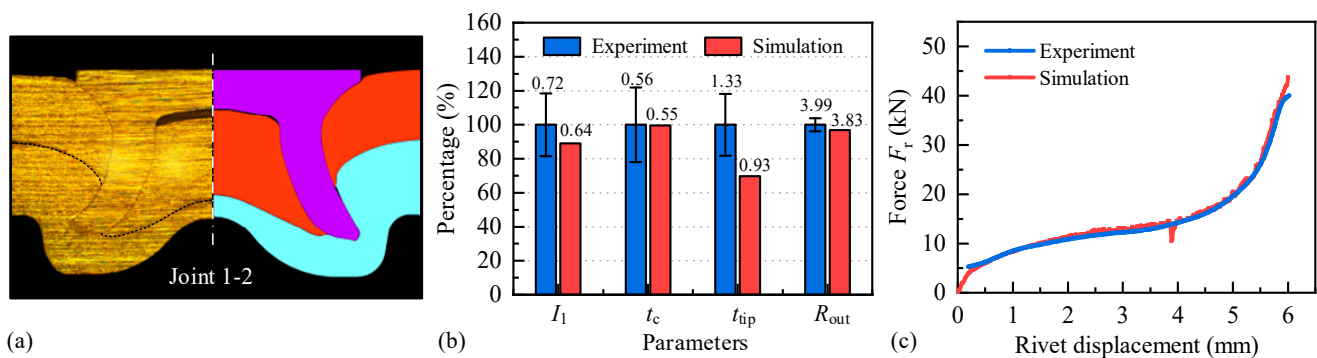


Figure 9. Comparisons of experimentally tested and simulated (a) cross-sectional profiles, (b) joint quality indicators and (c) force-displacement curves (in mm).

4.3. Impact of Friction Coefficients at Different Contact Interfaces

4.3.1. Between Rivet and Top Sheet (μ_1)

The simulated joint cross-sectional profiles with different μ_1 values are shown in Figure 10. It can be found that the deformed shapes of the rivet and sheets were apparently affected by the μ_1 . With the μ_1 increasing from 0.01 to 0.5, the inner and outer parts of the top sheet were stretched a greater distance towards the die cavity and underwent larger plastic deformation (see Figure 10e). This is because a higher friction force was generated at the rivet/top sheet interface with a larger μ_1 . The top sheet material surrounding the rivet shank was therefore dragged downward rather than rapidly penetrated. Due to the greater friction force, the rivet shank also underwent a larger plastic deformation with a larger μ_1 . The rivet shank flared outward but did not experience obvious upsetting when the μ_1 was 0.01, as shown in Figure 10a. Apparent rivet shank bulking occurred when the μ_1 increased to 0.5, as shown in Figure 10f. Owing to the alteration of rivet and top sheet deformation, the distribution of the remaining bottom sheet underneath the inner top sheet was also affected: less bottom sheet material was left underneath the rivet with a larger μ_1 (see Figure 10f). In addition, the filling condition of the rivet cavity was also influenced: it was fully filled with the $\mu_1 = 0.01$ but partially filled with a greater μ_1 .

Figure 11a shows the influence of μ_1 on the magnitude of I_1 . It can be seen that the I_1 demonstrates a rapid decline when the μ_1 increases from 0.01 to 0.5. A similar result was also obtained by Han et al. [11] through experimental tests, in which a smaller I_1 was achieved after the μ_1 was increased without applying E-coat on the top sheet surface. The E-coat can reduce the sheet surface roughness and thus provide some lubrication at the rivet/top sheet interface. To explain this phenomenon, the radius of inner (R_{in}) and outer (R_{out}) interlock boundaries (as shown in Figure 10a) that directly determine the I_1 value were measured, as shown in Figure 11b. The variation in μ_1 altered the rivet and sheet material deformation and thus influenced the two boundary positions. With the increment in μ_1 , the R_{in} kept almost constant and just fluctuated slightly. In contrast, the R_{out} rapidly declined from about 3.9 to 3.6 mm. This is attributed to greater deformation and even bulking of the rivet shank with a larger μ_1 , as shown in Figure 12. Severe plastic

deformation of the rivet shank was also reported by Hoang et al. [23] after increasing the friction coefficient between rivet/sheets from 0.0 to 0.8. The different changing trends of R_{in} and R_{out} indicate that the μ_1 influences the magnitude of I_1 by affecting the position of the outer interlock boundary. The changing trends of t_c and t_{tip} with different μ_1 values are shown in Figure 11c. The t_c shows a decreasing tendency with the μ_1 increasing from 0.01 to 0.5. The t_{tip} demonstrates a complex fluctuation: it first increases and then slowly decreases followed by an increment. This is because the magnitude of t_{tip} is determined by both the flaring distance along the radial direction and bulking degree of the rivet shank.

The μ_1 also imposed significant influences on the force-displacement curves, as shown in Figure 11d. At the early stage, almost the same riveting force (Zone 1) was observed with different μ_1 values. This is because only a small part of the rivet shank was inserted into the top sheet. The variation in friction force induced by the μ_1 was too small to cause distinct differences in the riveting force. However, with further increment in rivet displacement, a higher riveting force was observed with the increment in μ_1 (Zone 2). At this stage, a larger part of the rivet shank pierced into the top sheet, and the friction force at the rivet/top sheet interface accounted for a large portion of the riveting force. As a result, the riveting force became sensitive to the magnitude of μ_1 and reached a higher level with the increment in μ_1 . Changes in the rivet and sheet deformation also caused a faster filling speed of the die cavity space, which led to a larger riveting force. At the end of the joining process, differences in riveting force became smaller and the maximum riveting force values were very close (Zone 3).

From the above results, it can be concluded the friction coefficient at rivet/top sheet interface has significant influences on the I_1 , remaining bottom sheet thickness and riveting force. To achieve a high-quality SPR joint, it is recommended to reduce this friction coefficient by applying coatings (e.g., zinc/tin or zinc/tin/aluminium [5]) or lubricants on the rivet shank. In addition, considering the apparent influence of μ_1 on the joining results, it will be better to identify the μ_1 value individually when developing an FE model for the SPR process.

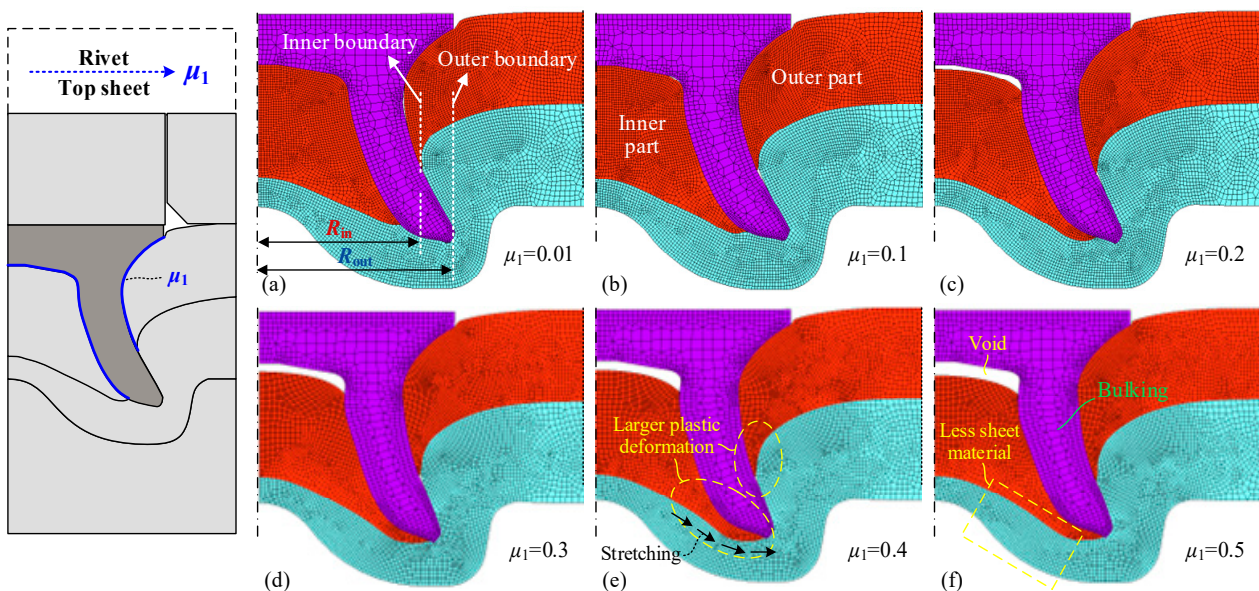


Figure 10. Simulated joint cross-sectional profiles with different friction coefficients between rivet and top sheet (μ_1): (a) $\mu_1=0.01$, (b) $\mu_1=0.1$, (c) $\mu_1=0.2$, (d) $\mu_1=0.3$, (e) $\mu_1=0.4$ and (f) $\mu_1=0.5$.

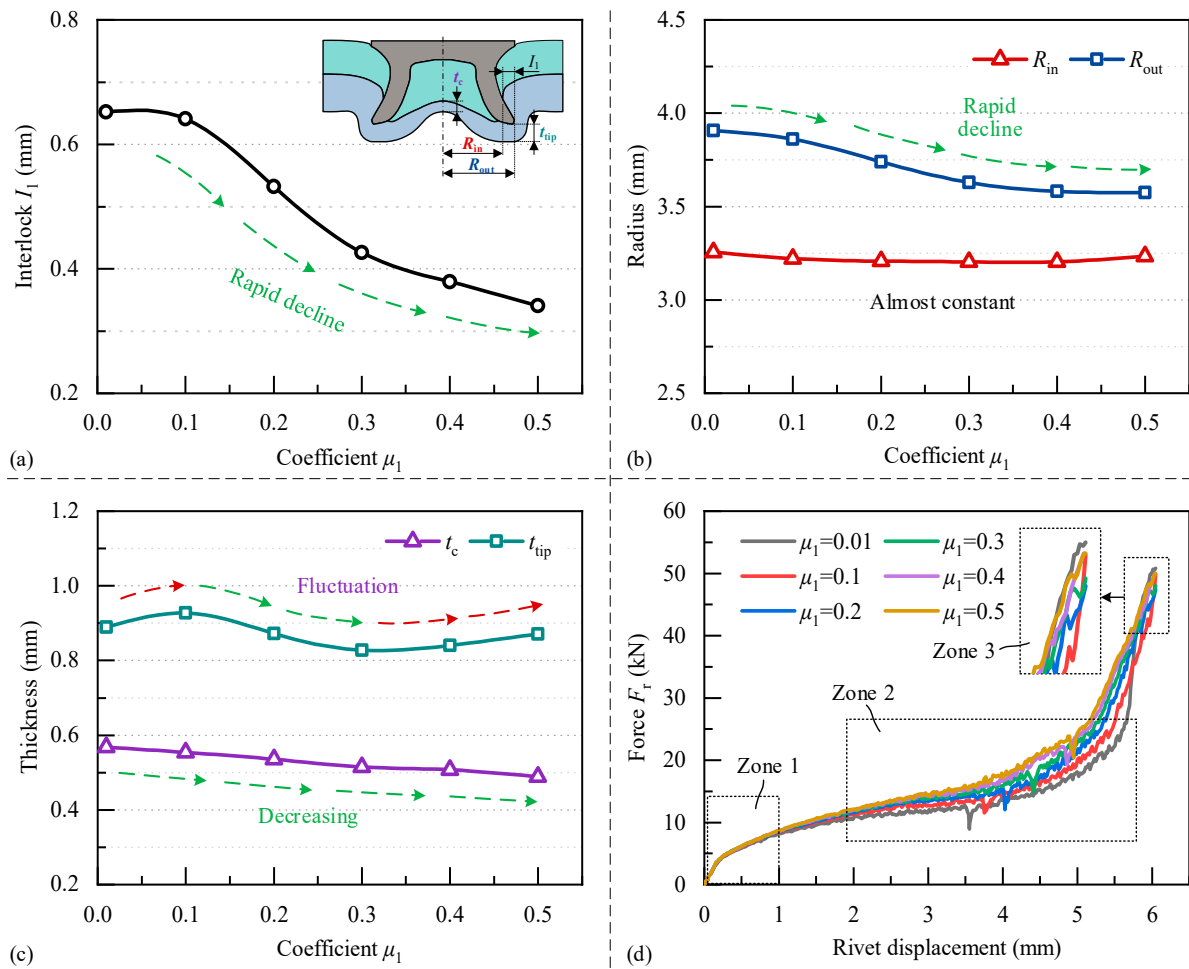


Figure 11. Variation trends of simulated (a) I_1 , (b) R_{in} and R_{out} , (c) t_c and t_{tip} , (d) force-displacement curves with different coefficient μ_1 values.

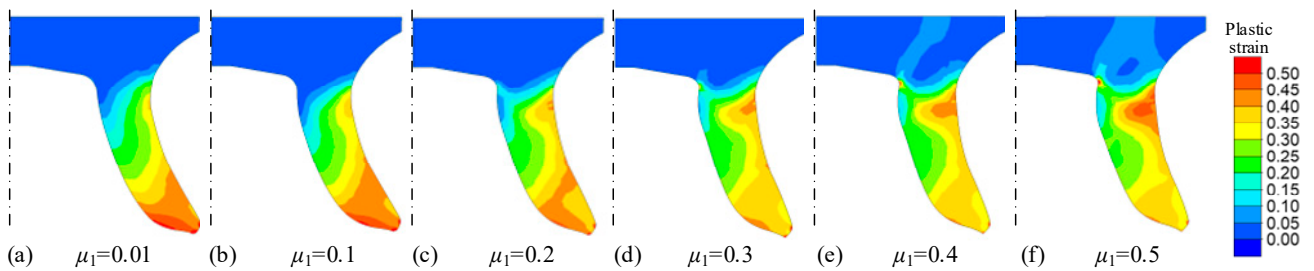


Figure 12. Plastic strain distributions on the rivet shank with different μ_1 values: (a) $\mu_1=0.01$, (b) $\mu_1 = 0.1$, (c) $\mu_1 = 0.2$, (d) $\mu_1 = 0.3$, (e) $\mu_1 = 0.4$ and (f) $\mu_1 = 0.5$.

4.3.2. Between Rivet and Bottom Sheet (μ_2)

Figure 13 shows the simulated joint cross-sectional profiles with different μ_2 values. Through visual observation, it is hard to distinguish the differences among these six joint profiles. This is because the μ_2 can only affect the joint formation after the rivet shank comes into contact with the bottom sheet. The limited impact of μ_2 on the joining result might be caused by the short interaction time and the small contact area between the rivet and bottom sheet.

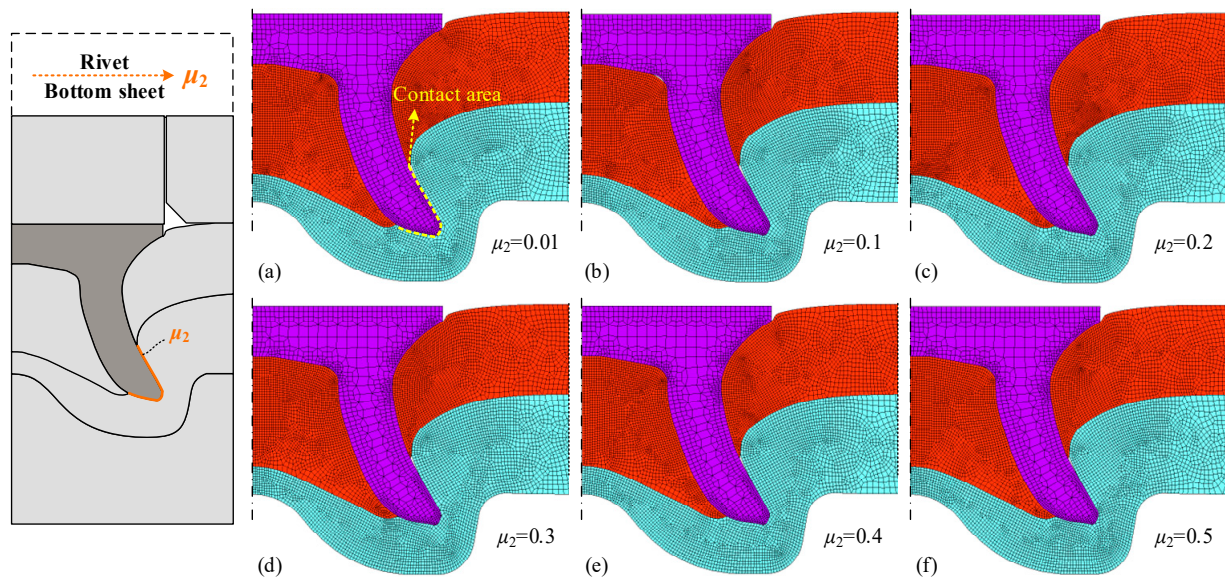


Figure 13. Simulated joint cross-sectional profiles with different friction coefficients between rivet and bottom sheet (μ_2): (a) $\mu_2 = 0.01$, (b) $\mu_2 = 0.1$, (c) $\mu_2 = 0.2$, (d) $\mu_2 = 0.3$, (e) $\mu_2 = 0.4$ and (f) $\mu_2 = 0.5$.

As shown in Figure 14a, the increment in the μ_2 imposes negative but not significant influences on the I_1 : it just slightly decreased with the μ_2 increasing from 0.01 to 0.5. Variation curves of the R_{in} and R_{out} are shown in Figure 14b. The almost constant values indicate that the μ_2 has limited impacts on the positions of left and right interlock boundaries. Meanwhile, change in the I_1 was not dominated by R_{in} or R_{out} alone, but a comprehensive effect of the R_{in} and R_{out} . Figure 14c shows the changing trends of t_c and t_{tip} with different μ_2 values. It can be seen that the t_c kept almost constant and was nearly not affected by the μ_2 . This is because the formation of t_c mainly occurs at the stage of rivet shank piercing through the top sheet [38]. In contrast, the t_{tip} shows an increasing trend with the increment in the μ_2 . This might be because the greater friction force at the rivet shank/bottom sheet interface restricted the rivet shank piercing into the bottom sheet. As a result, the rivet tip was slightly upset and led to a greater t_{tip} . Figure 14d shows the force-displacement curves with different μ_2 values. It can be seen that the change in μ_2 imposed very limited influences on the riveting force. Unsurprisingly, an identical riveting force (Zone 1) was observed before the top sheet was completely penetrated. Minor differences in riveting force were captured when the rivet shank gradually pierced into the bottom sheet (Zone 2). The maximum riveting force was almost the same on the six curves.

Overall, the friction coefficient at the rivet/bottom sheet interface can affect the I_1 and remaining bottom sheet thickness but impose limited influences on the riveting force. Because of surface abrasion when the rivet shank pierces through the top sheet, coating shedding or surface quality degradation of the rivet shank usually happens [14]. For top and bottom sheets with the same material and surface conditions, the μ_2 will be undoubtedly greater than the μ_1 . In addition, considering the lower influence of μ_2 on the joining result, an equal or slightly larger μ_2 is recommended compared with the μ_1 when developing an FE model for the SPR process. The μ_2 could be identified at the same time as the μ_1 rather than identified individually.

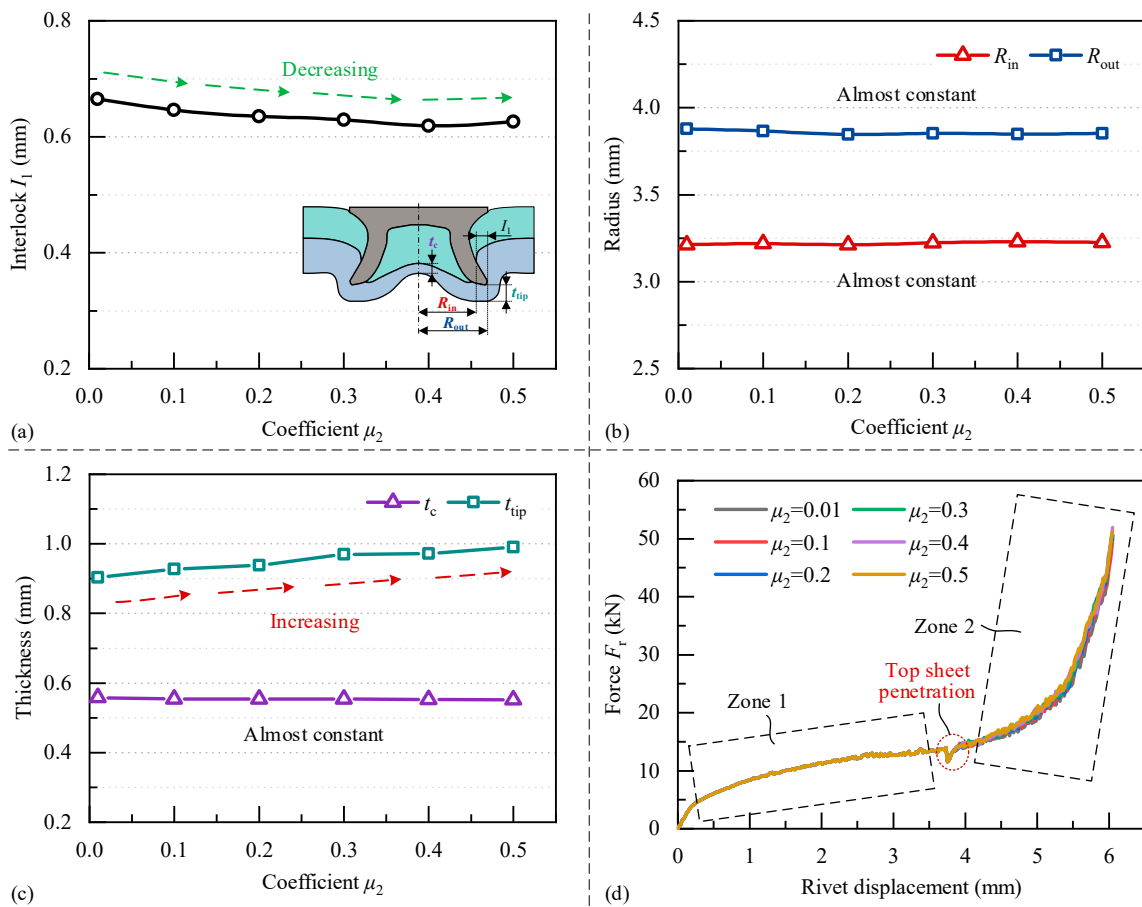


Figure 14. Variation trends of simulated (a) I_1 , (b) R_{in} and R_{out} , (c) t_c and t_{tip} , (d) force-displacement curves with different coefficient μ_2 values.

4.3.3. Between Top and Bottom Sheets (μ_3)

The simulated joint cross-sectional profiles with different μ_3 values are shown in Figure 15. It can be seen that the filling condition of the rivet cavity was apparently affected by the μ_3 : the rivet cavity was fully filled with $\mu_3 = 0.01$ as shown in Figure 15a but not filled up with $\mu_3 = 0.5$ as shown in Figure 15f. This is because the inner part of the top sheet applied higher friction force on the bottom sheet, which facilitated the material flow of the bottom sheet from the joint centre to the die cavity. As a result, more bottom sheet material was accumulated in the die cavity (Zone 1 vs. Zone 2) and less sheet material was trapped in the rivet cavity with a greater μ_3 . Due to changes in the bottom sheet deformation behaviour and rivet cavity filling condition, the deformed profile of the rivet shank was also affected: the rivet shank flared a larger distance along the radial direction with a greater μ_3 but experienced slight upsetting as shown in Figure 15f.

As shown in Figure 16a, the I_1 first rises with the μ_3 increasing from 0.01 to 0.4 but then decreases with the μ_3 further increasing to 0.5. With the increment in μ_3 , both R_{in} and R_{out} show increasing tendencies, as shown in Figure 16b, and work together to determine the changing trend of I_1 . Figure 16c shows the variation trends of t_c and t_{tip} with the μ_3 from 0.01 to 0.5. It can be seen that the μ_3 shows opposite influences on the t_c and t_{tip} : the t_c demonstrates a decreasing trend whilst the t_{tip} rapidly increases with the increment in μ_3 . With a greater μ_3 , a larger friction force was generated at the top/bottom sheet interface and caused a stronger stretching effect on the bottom sheet material at the joint centre, which directly caused the reduction in t_c . The increment in t_{tip} is a comprehensive result of greater rivet shank flaring and upsetting. Force-displacement curves with different μ_3 values are shown in Figure 16d. The μ_3 shows very limited influences on the magnitudes

of the riveting force (Zone 1), and apparent differences were only observed at the end of the joining processes (Zone 2). The maximum riveting force shows a declining trend with the increment in μ_3 .

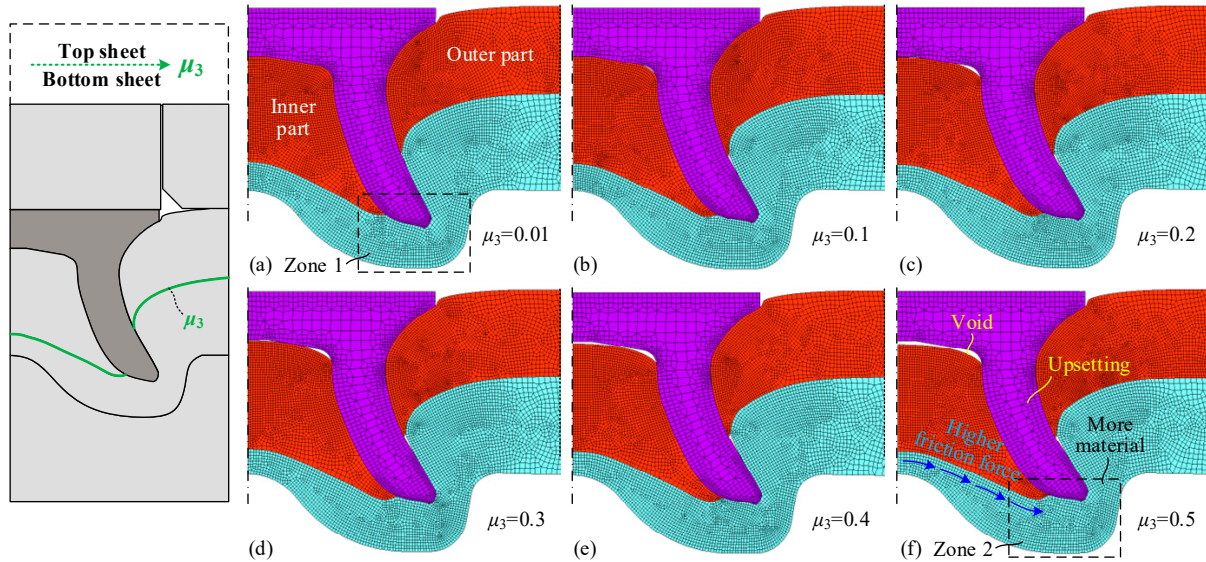


Figure 15. Simulated joint cross-sectional profiles with different friction coefficients between top and bottom sheets (μ_3): (a) $\mu_3 = 0.01$, (b) $\mu_3 = 0.1$, (c) $\mu_3 = 0.2$, (d) $\mu_3 = 0.3$, (e) $\mu_3 = 0.4$ and (f) $\mu_3 = 0.5$.

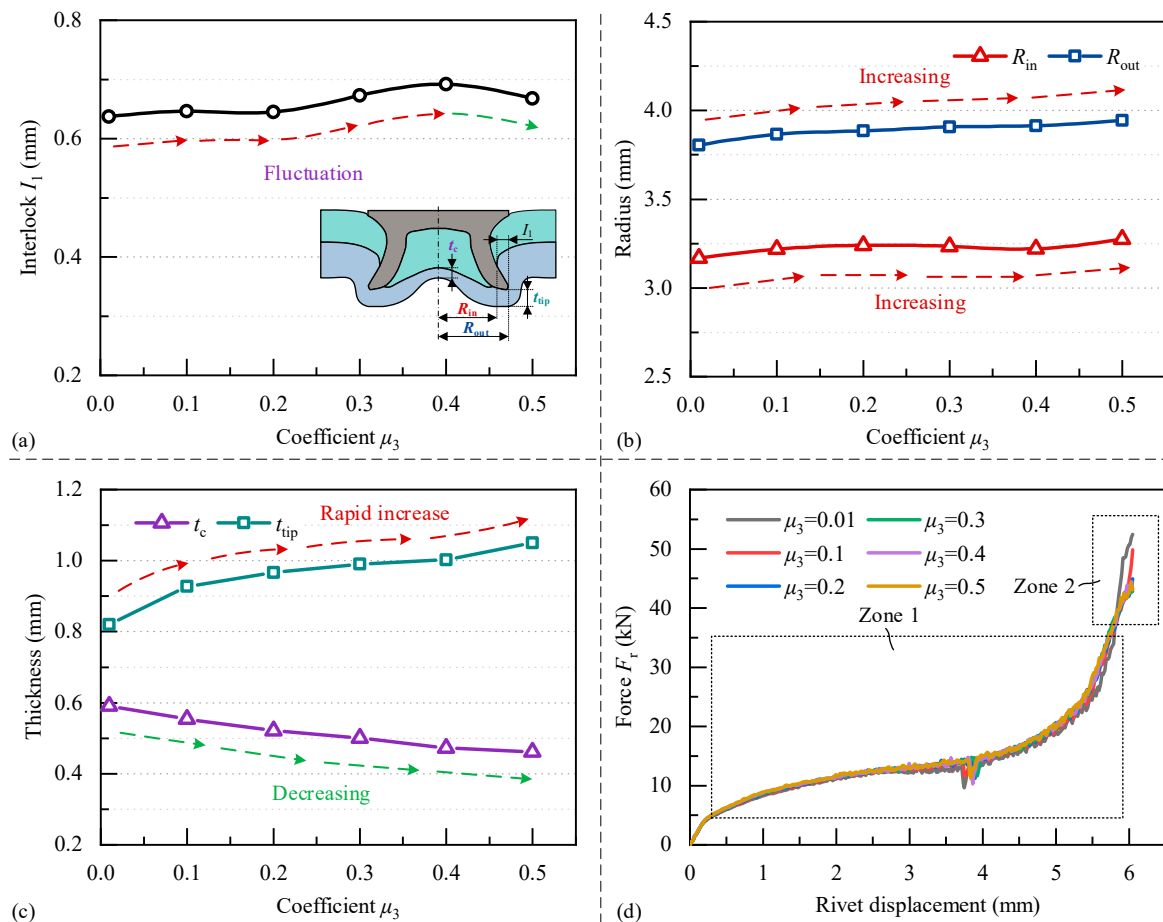


Figure 16. Variation trends of simulated (a) I_1 , (b) R_{in} and R_{out} , (c) t_c and t_{tip} , (d) force-displacement curves with different coefficient μ_3 values.

In practice, many factors will influence the friction coefficient at the top/bottom sheet interface. For example, lubricants applied on the sheet surface during the rolling process [39] or the stamping process [13] will impose a lubrication effect and result in a smaller μ_3 . The application of liquid adhesive at a two-sheet interface may also have a lubrication effect [5]. As a result, the joint quality would be slightly changed. Considering its apparent influences on the t_c and t_{tip} , it is recommended to tune and identify the μ_3 individually when developing an FE model for the SPR process.

4.3.4. Between Bottom Sheet and Die (μ_4)

The simulated joint cross-sectional profiles with different μ_4 values are shown in Figure 17. It can be found that the deformed shapes of the rivet and sheets, especially the bottom sheet, were apparently affected by the μ_4 . This agrees well with the simulation results reported by Moraes et al. [20], in which the significant impact of the μ_4 on joint formation and final quality was highlighted. With the increment in μ_4 , the inner part of the top sheet underwent larger deformation (see Figure 17f). Instead, the inner top sheet was deformed and stretched by the rivet shank. The outer part of the top sheet achieved very similar deformation and was less affected by the μ_4 . For the bottom sheet, more sheet material was left at the joint central area with a greater μ_4 (see Figure 17e). This is directly caused by the greater friction force at the bottom sheet/die interface, which resisted the flow of bottom sheet material into the die cavity. Slight rivet shank upsetting was observed with the $\mu_4 = 0.01$, as shown in Figure 17a. This is because a large amount of sheet material underneath the rivet cavity was pressed into the die cavity. The fully filled die cavity but unfilled rivet cavity directly led to the upsetting of the rivet shank. With the increment in μ_4 , less sheet material was pressed into the die cavity, which alleviated the hostile filling states of rivet and die cavities for rivet shank stability and therefore avoided apparent rivet shank upsetting, as shown in Figure 17f.

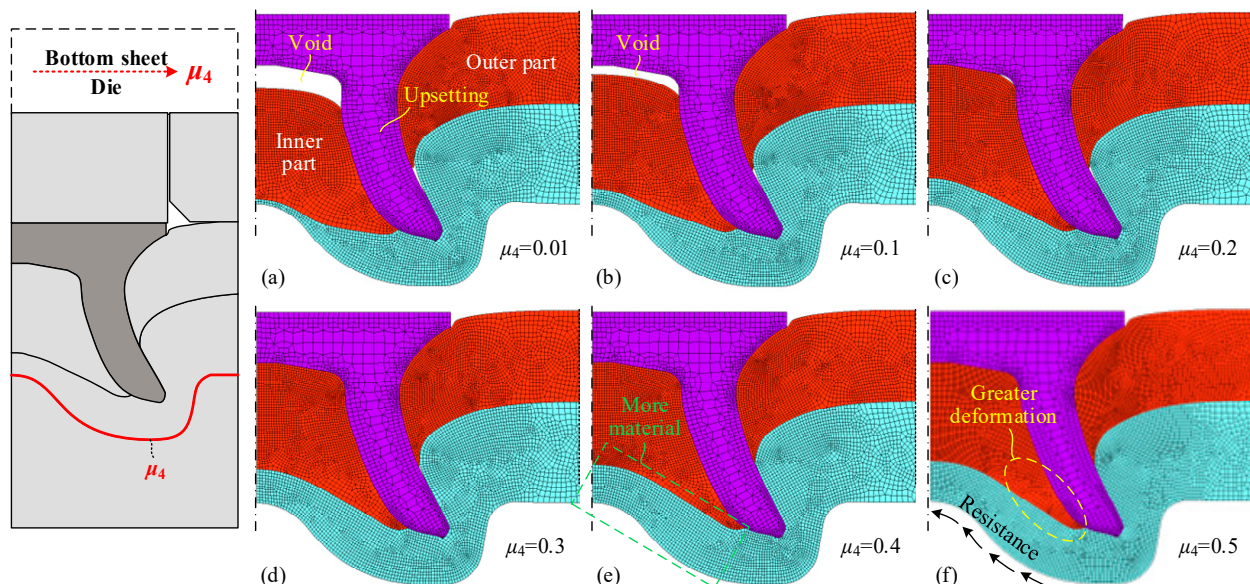


Figure 17. Simulated joint cross-sectional profiles with different friction coefficients between bottom sheet and die (μ_4): (a) $\mu_4 = 0.01$, (b) $\mu_4 = 0.1$, (c) $\mu_4 = 0.2$, (d) $\mu_4 = 0.3$, (e) $\mu_4 = 0.4$ and (f) $\mu_4 = 0.5$.

As shown in Figure 18a, the I_1 fluctuated within a narrow range when the μ_4 increased from 0.01 to 0.5. Both R_{in} and R_{out} demonstrated increasing trends with the increment in μ_4 in Figure 18b. This is because less bottom sheet material was accumulated outside the rivet shank, which led to lower resistance on the outer surface of the rivet shank. The larger amount of sheet material accumulated in the rivet cavity imposed a stronger guidance effect on the rivet shank flaring [6]. Thus, the rivet shank flared a greater distance along the radial

direction and resulted in a greater radius of inner and outer interlock boundaries. Variation trends of the t_c and t_{tip} with different μ_4 values are shown in Figure 18c. It can be seen that the t_c was significantly affected by the μ_4 and rapidly increased from around 0.08 mm to 0.80 mm. As aforementioned, this is also directly caused by the accumulation of bottom sheet material at the joint centre, induced by greater friction forces at the bottom sheet/die interface. In contrast, the t_{tip} was less influenced and kept almost constant with varying μ_4 , which is a result of the comprehensive effects of rivet shank upsetting and flaring. In addition, from the cross-sectional profiles in Figure 17, it is also worth mentioning that the μ_4 is capable of controlling the thickness distribution of the bottom sheet. A proper μ_4 can produce a reasonable bottom sheet thickness distribution and therefore increase the joint strength and reliability to prevent corrosion. Figure 18d shows the force-displacement curves with different μ_4 values. At the early stage of the joining processes, the riveting force was just slightly affected by the μ_4 (Zone 1). An obvious difference in the riveting force was observed at the end of the joining processes (Zone 2): the bigger the μ_4 , the larger the riveting force. Moreover, the maximum riveting force demonstrated an increasing trend with the increment in μ_4 from 0.01 to 0.5.

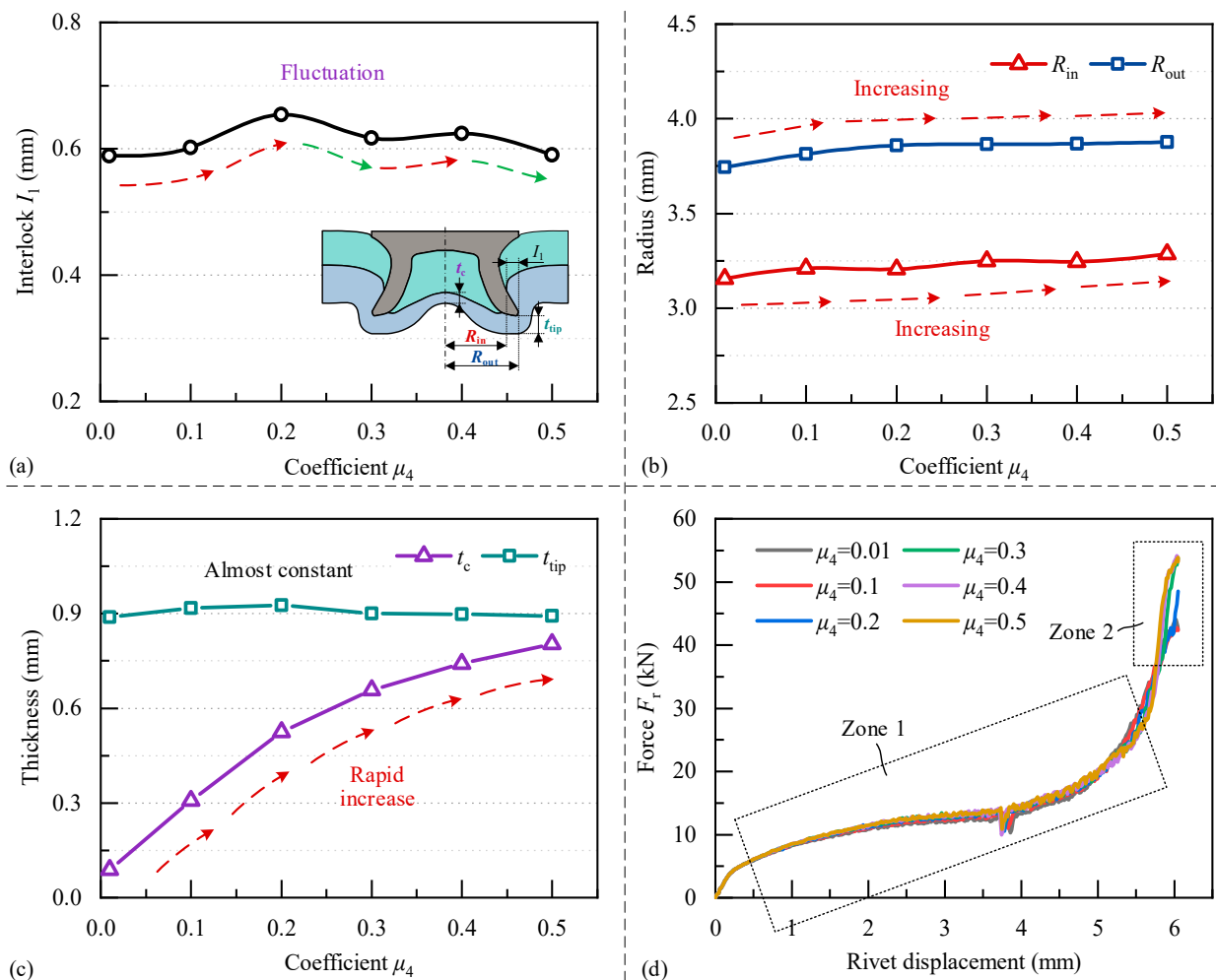


Figure 18. Variation trends of simulated (a) I_1 , (b) R_{in} and R_{out} , (c) t_c and t_{tip} , (d) force-displacement curves with different coefficient μ_4 values.

From the above discussion, it can be concluded that the friction coefficient at the bottom sheet/die interface has crucial influences on the joining results, especially the thickness distribution of the bottom sheet. Coatings or lubricants applied on the bottom sheet or die are helpful for rivet shank flaring but will inevitably reduce the remaining bottom

sheet material at the joint centre. In contrast, the wear of the die in service will increase the magnitude of μ_4 and impose opposite influences on the joining results. Considering its significant influences, the μ_4 should be identified individually when developing an FE model for the SPR process.

From the above results, it can be found that the four friction coefficients demonstrate different degrees of impact on the joint quality indicators. For easier comparison, the changing trends of I_1 , R_{in} , R_{out} , t_c and t_{tip} are summarised in Table 4. The μ_1 shows the greatest influence on the I_1 , whilst the μ_4 demonstrates the greatest impact on the t_c . Both μ_1 and μ_3 impose critical but opposite influences on R_{out} by affecting the rivet shank flaring behaviour. The μ_3 demonstrates greater effects on t_{tip} than the other three friction coefficients. Compared with other quality indicators, the variations in friction coefficients impose the lowest influence on the R_{in} . Overall, altering the friction coefficients at different contact interfaces through coatings, lubricating oil or other strategies is effective and promising for improving SPR joint quality in practice.

Table 4. Comparisons of four different coefficients’ influences on joint quality indicators.

Friction Coefficient		I_1	R_{in}	R_{out}	t_c	t_{tip}
Rivet/top sheet (μ_1)	↑	↓↓	↔	↓↓	↓	~~
Rivet/bottom sheet (μ_2)	↑	↓	↔	↔	↔	↑
Top/bottom sheets (μ_3)	↑	~~	↑	↑↑	↓	↑↑
Bottom sheet/die (μ_4)	↑	~~	↑	↑	↑↑	↔

Note: (1) increase ↑; (2) rapid increase ↑↑; (3) decrease ↓; (4) rapid decrease ↓↓; (5) fluctuation ~~; (6) almost constant ↔.

5. Conclusions

In this study, the impacts of surface conditions/friction coefficients at different contact interfaces on SPR joint quality were experimentally and numerically investigated. The main conclusions are as follows:

- (1) Reducing the friction coefficient between the rivet and top sheet (μ_1) by applying coatings or lubricating oil on the rivet can effectively increase the magnitudes of interlock (I_1) and remaining bottom sheet thickness at the joint centre (t_c). The joining force can also be reduced with a greater μ_1 , providing the benefits of less energy consumption and longer service life of the die.
- (2) The joint quality was less affected by the friction coefficient between the rivet and bottom sheet (μ_2). In practice, reducing the magnitude of μ_2 by rivet coating or other strategies can slightly increase the I_1 without imposing apparent influences on the t_c and riveting force.
- (3) Increasing the friction coefficient between top and bottom sheets (μ_3) can lead to a greater rivet shank flaring distance. The μ_3 imposes opposite influences on the t_{tip} and t_c and therefore can be adjusted by modifying the contact surface condition to balance the magnitudes of the t_{tip} and t_c for better joint quality.
- (4) The friction coefficient between the bottom sheet and die (μ_4) imposes a critical impact on the magnitude of the t_c by affecting the bottom sheet deformation behaviour. Reducing the μ_4 by applying lubricating oil at the bottom sheet/die interface or increasing the μ_4 with a rougher die surface can reduce or increase the t_c to optimise the joint quality.
- (5) Among the four friction coefficients at contact interfaces, the μ_1 and μ_4 impose greater influences on the magnitudes of joint quality indicators. The identified changing trends of I_1 , R_{out} , t_{tip} and t_c with varying friction coefficients are beneficial for a quick selection of friction coefficients with the inverse method in FE model development process.

Author Contributions: Conceptualisation, H.Z.; methodology, H.Z.; visualisation, Y.L.; writing—original draft preparation, H.Z. and Y.L.; writing—review and editing, H.Z. and Y.L.; supervision, L.H. and X.L.; project administration, X.L. All authors have read and agreed to the published version of the manuscript.

Funding: This research was funded by Jaguar Land Rover, the National Natural Science Foundation of China (Grant No. 52205397) and the China Postdoctoral Science Foundation (Grant No. 2022M722083).

Institutional Review Board Statement: Not applicable.

Informed Consent Statement: Not applicable.

Data Availability Statement: The data presented in this study are available on request from the corresponding author.

Acknowledgments: The authors would like to thank Matthias Wissling, Paul Bartig and their team members from Tucker GmbH for their support during the laboratory tests.

Conflicts of Interest: The authors declare no conflict of interest.

References

1. Miller, W.S.; Zhuang, L.; Bottema, J.; Wittebrood, A.J.; De Smet, P.; Haszler, A.; Vieregge, A. Recent development in aluminium alloys for the automotive industry. *Mater. Sci. Eng. A* **2000**, *280*, 37–49. [\[CrossRef\]](#)
2. Mortimer, J. Jaguar Uses X350 Car to Pioneer Use of Self-Piercing Rivets. *Ind. Robot An Int. J.* **2001**, *28*, 192–198. [\[CrossRef\]](#)
3. Hewitt, R. Self-Piercing Riveting (SPR) in Automated Vehicle Construction. In *Self-Piercing Riveting: Properties, Processes and Applications*; Woodhead Publishing: Sawston, Cambridge, UK, 2014; pp. 181–207. ISBN 9781845695354.
4. Abe, Y.; Kato, T.; Mori, K. Self-Piercing Riveting of High Tensile Strength Steel and Aluminium Alloy Sheets Using Conventional Rivet and Die. *J. Mater. Process. Technol.* **2009**, *209*, 3914–3922. [\[CrossRef\]](#)
5. Li, D.; Chrysanthou, A.; Patel, I.; Williams, G. Self-Piercing Riveting-vA Review. *Int. J. Adv. Manuf. Technol.* **2017**, *92*, 1777–1824. [\[CrossRef\]](#)
6. Liu, Y.; Li, H.; Zhao, H.; Liu, X. Effects of the Die Parameters on the Self-Piercing Riveting Process. *Int. J. Adv. Manuf. Technol.* **2019**, *105*, 3353–3368. [\[CrossRef\]](#)
7. Haque, R.; Beynon, J.H.; Durandet, Y. Characterisation of Force-Displacement Curve in Self-Pierce Riveting. *Sci. Technol. Weld. Join.* **2012**, *17*, 476–488. [\[CrossRef\]](#)
8. Wakuda, M.; Yamauchi, Y.; Kanzaki, S.; Yasuda, Y. Effect of Surface Texturing on Friction Reduction between Ceramic and Steel Materials under Lubricated Sliding Contact. *Wear* **2003**, *254*, 356–363. [\[CrossRef\]](#)
9. Han, S.L.; Tang, X.D.; Gao, Y.; Zeng, Q.L. Effects of Friction Factors on Flat Bottom Self-Pierce Riveting Joints of AZ31 Magnesium Alloy. *Mater. Res. Innov.* **2015**, *19*, S10-235–S10-238. [\[CrossRef\]](#)
10. Li, D. Influence of Aluminium Sheet Surface Modification on the Self-Piercing Riveting Process and the Joint Static Lap Shear Strength. *Int. J. Adv. Manuf. Technol.* **2017**, *93*, 2685–2695. [\[CrossRef\]](#)
11. Han, L.; Chrysanthou, A. Evaluation of Quality and Behaviour of Self-Piercing Riveted Aluminium to High Strength Low Alloy Sheets with Different Surface Coatings. *Mater. Des.* **2008**, *29*, 458–468. [\[CrossRef\]](#)
12. Li, D. Influence of Local Surface Texture by Tool Impression on the Self-Piercing Riveting Process and the Static Lap Shear Strength. *J. Manuf. Process.* **2017**, *29*, 298–309. [\[CrossRef\]](#)
13. Lovell, M.; Higgs, C.F.; Deshmukh, P.; Mobley, A. Increasing Formability in Sheet Metal Stamping Operations Using Environmentally Friendly Lubricants. *J. Mater. Process. Technol.* **2006**, *177*, 87–90. [\[CrossRef\]](#)
14. Karim, M.A.; Jeong, T.E.; Noh, W.; Park, K.Y.; Kam, D.H.; Kim, C.; Nam, D.G.; Jung, H.; Park, Y. Do Joint Quality of Self-Piercing Riveting (SPR) and Mechanical Behavior under the Frictional Effect of Various Rivet Coatings. *J. Manuf. Process.* **2020**, *58*, 466–477. [\[CrossRef\]](#)
15. Uhe, B.; Kuball, C.M.; Merklein, M.; Meschut, G. Influence of the Rivet Coating on the Friction during Self-Piercing Riveting. *Key Eng. Mater.* **2021**, *883*, 11–18. [\[CrossRef\]](#)
16. Rossel, M.; Meschut, G. Investigation of the Friction Conditions of Self-Pierce Rivets by Means of a Compression-Torsion Tribometer. *Prod. Eng.* **2022**, *16*, 673–682. [\[CrossRef\]](#)
17. Tassler, T.; Israel, M.; Goede, M.F.; Dilger, K.; Dröder, K. Robust Joining Point Design for Semi-Tubular Self-Piercing Rivets. *Int. J. Adv. Manuf. Technol.* **2018**, *98*, 431–440. [\[CrossRef\]](#)
18. Zhao, H.; Han, L.; Liu, Y.; Liu, X. Modelling and Interaction Analysis of the Self-Pierce Riveting Process Using Regression Analysis and FEA. *Int. J. Adv. Manuf. Technol.* **2021**, *113*, 159–176. [\[CrossRef\]](#)
19. Carandente, M.; Dashwood, R.J.; Masters, I.G.; Han, L. Improvements in Numerical Simulation of the SPR Process Using a Thermo-Mechanical Finite Element Analysis. *J. Mater. Process. Technol.* **2016**, *236*, 148–161. [\[CrossRef\]](#)
20. Moraes, J.F.C.; Jordon, J.B.; Ilieva, E.I. Influence of the Friction Coefficient in Self-Pierce Riveting Simulations: A Statistical Analysis. *SAE Int. J. Mater. Manuf.* **2018**, *11*, 123–130. [\[CrossRef\]](#)
21. Huang, L.; Wu, Y.; Huff, G.; Huang, S.; Ilinich, A.; Freis, A.; Luckey, G. Sensitivity Study of Self-Piercing Rivet Insertion Process Using Smoothed Particle Galerkin Method. *16th Int. LS-DYNA Users Conf.* **2020**, 1–11.

22. Mucha, J. A Study of Quality Parameters and Behaviour of Self-Piercing Riveted Aluminium Sheets with Different Joining Conditions. *Stroj. Vestn. J. Mech. Eng.* **2011**, *57*, 323–333. [[CrossRef](#)]
23. Hoang, N.H.; Hopperstad, O.S.; Langseth, M.; Westermann, I. Failure of Aluminium Self-Piercing Rivets: An Experimental and Numerical Study. *Mater. Des.* **2013**, *49*, 323–335. [[CrossRef](#)]
24. Han, L.; Chrysanthou, A.; O’Sullivan, J.M. Fretting Behaviour of Self-Piercing Riveted Aluminium Alloy Joints under Different Interfacial Conditions. *Mater. Des.* **2006**, *27*, 200–208. [[CrossRef](#)]
25. Wituschek, S.; Kuball, C.M.; Merklein, M.; Lechner, M. Test Method for Friction Characterization of Rivets. *Defect Diffus. Forum* **2020**, *404 DDF*, 132–137. [[CrossRef](#)]
26. Wang, X.; Wang, C.; Mu, R. Numerical Simulation and Experimental Study on Self-Piercing Riveting of DC03 / 6016 Dissimilar Sheets. In Proceedings of the International Conference on Electron Device and Mechanical Engineering, Suzhou, China, 1–3 May 2020; pp. 463–466.
27. Karathanasopoulos, N.; Pandya, K.S.; Mohr, D. Self-Piercing Riveting Process: Prediction of Joint Characteristics through Finite Element and Neural Network Modeling. *J. Adv. Join. Process.* **2021**, *3*, 100040. [[CrossRef](#)]
28. Deng, J.H.; Lyu, F.; Chen, R.M.; Fan, Z.S. Influence of Die Geometry on Self-Piercing Riveting of Aluminum Alloy AA6061-T6 to Mild Steel SPFC340 Sheets. *Adv. Manuf.* **2019**, *7*, 209–220. [[CrossRef](#)]
29. Rusia, A.; Weihe, S. Development of an End-to-End Simulation Process Chain for Prediction of Self-Piercing Riveting Joint Geometry and Strength. *J. Manuf. Process.* **2020**, *57*, 519–532. [[CrossRef](#)]
30. Hönsch, F.; Domitner, J.; Sommitsch, C.; Götzinger, B. Modeling the Failure Behavior of Self-Piercing Riveting Joints of 6xxx Aluminum Alloy. *J. Mater. Eng. Perform.* **2020**, *29*, 4888–4897. [[CrossRef](#)]
31. Moraes, J.F.C.; Jordon, J.B.; Su, X.; Barkey, M.E.; Jiang, C.; Ilieva, E. Effect of Process Deformation History on Mechanical Performance of AM60B to AA6082 Self-Pierce Riveted Joints. *Eng. Fract. Mech.* **2019**, *209*, 92–104. [[CrossRef](#)]
32. Amro, E.; Kouadri-Henni, A. Joining of Polymer-Metal Lightweight Structures Using Self-Piercing Riveting (SPR) Technique: Numerical Approach and Simulation Results. In Proceedings of the AIP Conference Proceedings, Palermo, Italy, 23–25 April 2018; Volume 1960, p. 050001.
33. Huang, L.; Guo, H.; Shi, Y.; Huang, S.; Su, X. Fatigue Behavior and Modeling of Self-Piercing Riveted Joints in Aluminum Alloy 6111. *Int. J. Fatigue* **2017**, *100*, 274–284. [[CrossRef](#)]
34. Hirsch, F.; Müller, S.; Machens, M.; Staschko, R.; Fuchs, N.; Kästner, M. Simulation of Self-Piercing Riveting Processes in Fibre Reinforced Polymers: Material Modelling and Parameter Identification. *J. Mater. Process. Technol.* **2017**, *241*, 164–177. [[CrossRef](#)]
35. He, X.; Xing, B.; Zeng, K.; Gu, F.; Ball, A. Numerical and Experimental Investigations of Self-Piercing Riveting. *Int. J. Adv. Manuf. Technol.* **2013**, *69*, 715–721. [[CrossRef](#)]
36. Han, L.; Thornton, M.; Shergold, M. A Comparison of the Mechanical Behaviour of Self-Piercing Riveted and Resistance Spot Welded Aluminium Sheets for the Automotive Industry. *Mater. Des.* **2010**, *31*, 1457–1467. [[CrossRef](#)]
37. Liu, Y.; Han, L.; Zhao, H.; Liu, X. Evaluation and Correction of Cutting Position’s Effects on Quality Indicator Measurement of Self-Piercing Riveted Joint. *Mater. Des.* **2021**, *202*, 109583. [[CrossRef](#)]
38. Zhao, H.; Han, L.; Liu, Y.; Liu, X. Analysis of Joint Formation Mechanisms for Self-Piercing Riveting (SPR) Process with Varying Joining Parameters. *J. Manuf. Process.* **2022**, *73*, 668–685. [[CrossRef](#)]
39. Schmid, S.R.; Wilson, W.R.D. Lubrication of Aluminum Rolling by Oil-in-Water Emulsions. *Tribol. Trans.* **1995**, *38*, 452–458. [[CrossRef](#)]

Disclaimer/Publisher’s Note: The statements, opinions and data contained in all publications are solely those of the individual author(s) and contributor(s) and not of MDPI and/or the editor(s). MDPI and/or the editor(s) disclaim responsibility for any injury to people or property resulting from any ideas, methods, instructions or products referred to in the content.